Applied Materials Today 15 (2019) 323–334

Contents lists available at ScienceDirect

Applied Materials Today

journal homepage: www.elsevier.com/locate/apmt

Cu nanoclusters in ion exchanged soda-lime glass: Study of SPR and nonlinear optical behavior for photonics

Promod Kumar[a,*], Mohan Chandra Mathpal[b], Syed Hamad[c], Soma Venugopal Rao[c], J.H. Neethling[d], A. Janse van Vuuren[d], E.G. Njoroge[e,f], R.E. Kroon[a], W.D. Roos[a], H.C. Swart[a,*]

[a] Department of Physics, University of the Free State, Bloemfontein ZA9300, South Africa
[b] Department of Physics, Universidade de Brasília, Brasilia, DF 70910900, Brazil
[c] Advanced Centre for Research in High Energy Materials (ACRHEM), University of Hyderabad, Hyderabad, Telangana, India
[d] Centre for HRTEM, Nelson Mandela University, Port Elizabeth ZA6031, South Africa
[e] ENGAGE, University of Pretoria, Pretoria 0002, South Africa
[f] Department of Physics, University of Pretoria, Pretoria 0002, South Africa

ARTICLE INFO

Article history:
Received 2 December 2018
Received in revised form 13 February 2019
Accepted 21 February 2019

Keywords:
Structural
Nanoparticles
Surface plasmon resonance
Metal forming and shaping
Z-scan technique

ABSTRACT

Nanomaterials with large optical nonlinearities have received considerable attention in the field of modern science and nanotechnology. In this paper, we have studied nonlinear optical and surface plasmon resonance properties and behavior of Cu nanoclusters formed in ion exchanged soda-lime glass. The soda-lime glasses were successfully doped with Cu nanoclusters in the ion-exchange process. The size of the clusters estimated from the optical absorption spectroscopy results closely matched with those obtained from the transmission electron microscopy data. The results revealed that spherical shaped Cu nanoclusters were homogeneously distributed in the glass matrix and the size of the Cu nanoclusters varied from 4 to 10 nm. The structure and chemical state were further analyzed by X-ray diffraction and X-ray photoelectron spectroscopy. The nonlinear optical behavior of the materials was analyzed using femtosecond Z-scan technique. The nonlinear refraction index γ, nonlinear absorption coefficient β and the third-order nonlinear optical susceptibility $\chi^{(3)}$ were estimated to be -1.72×10^{-17} m^2/W, 9.96×10^{-11} m/W, and 0.56×10^{-11} esu, respectively, which shows possible application in the field of photonics.

1. Introduction

In our modern era it is of the outmost importance to produce novel nano-photonic devices for the processing of data at high speeds and has been the motivation for investigating the properties of new nonlinear optical (NLO) materials. The focus on these new NLO materials is important for the progress of optical limiters for sensor protection [1], as mode-locking elements [2], and in optical switching devices [3], etc. When intense laser pulses are incident on glass materials doped with noble metals, NLO effects are exhibited beyond certain input peak intensities. Typically, nonlinear absorbers are classified into two categories named as reverse saturable absorbers (RSA) and saturable absorbers (SA) [4–8]. Recent studies demonstrate that plasmonic based hybrid nanostructures exhibit characteristics of SA, or RSA used mainly for optical limiter applications, and switching behavior (RSA in SA and SA in RSA) which can be accredited to the intra-band and inter-band transitions [9,10]. Plasmonic nanoparticles in dielectric media allow producing surface plasmons in the vicinity of dielectric surfaces resulting to the origin of a local evanescent field which experiences dielectric confinement. These fields affect the coherent oscillation of dipoles in the conduction band to enhance the yield of photons, hence enhancing the effective third order nonlinearity [11–13]. The strength of the nonlinearity is influenced by changing of the surface plasmon resonance (SPR) band and stability which could be possible due to the balancing of size and shape of the nanomaterials. Particularly, silver (Ag) and gold (Au) produce strong local evanescent fields which allow strengthening the ground state absorption cross-section during a single photon nonlinear process (SA) and also observed enhancement in the excited state's absorption cross-section during two photon processes (RSA) at higher peak intensities [4,5,14]. In the last few decades, scientists demonstrated that third-order NLO response of plasmonic based hybrid nanoclusters (NCs) has been influenced by host materials. For instance, plasmonic nanoparticles dispersed in a glass

* Corresponding authors.
E-mail addresses: talk2promodthakur@gmail.com (P. Kumar), SwartHC@ufs.ac.za (H.C. Swart).

https://doi.org/10.1016/j.apmt.2019.02.016
2352-9407/

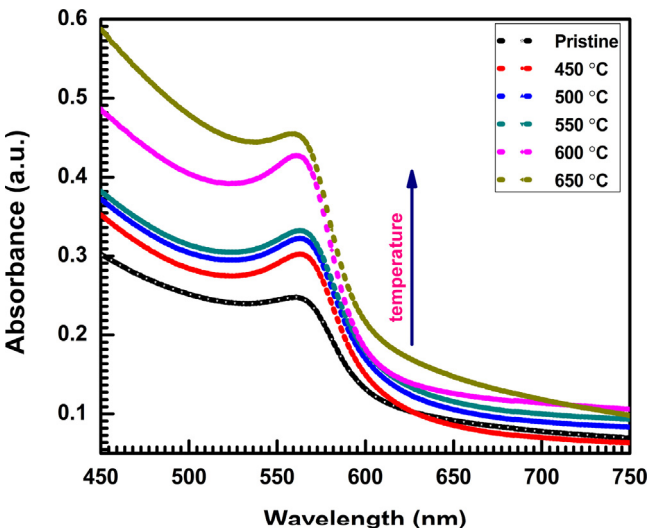

Fig. 1. Optical absorption spectra of Cu NCs formed in the glass matrix of pristine and annealed at various temperatures from 450 °C up to 650 °C.

host homogeneously which allowed control of the surface plasmon resonance properties. The NLO phenomena of noble metallic nanoparticles in a silica host were demonstrated by Fukumi in 1991 using a 532 nm wavelength and obtained a $\chi^{(3)}$ value of $\sim 10^{-7}$ e.s.u in the nanosecond domain [15]. Tsuji et al. [16] reported $\chi^{(3)}$ value of similar order ($\sim 10^{-7}$ esu) in the case of Cu doped soda-lime silicate glass. These values are orders of magnitude higher compared to the nonlinearity of a standard sample CS_2 ($\sim 10^{-12}$ esu) recorded with nanosecond pulses. Additionally, picosecond NLO properties of metal nanoparticles (Au, Ag and Cu) in SiO_2 matrix have been carried out in various spectral ranges by different research groups [16,17].

The choice of glass as a host material has many advantages, such as transparency in most of the band, good chemical stability and thermal stability, easy fiber forming and optical processing. There are several techniques mainly used to synthesize noble metal nanoparticles in a glass matrix, such as the melting method, ion injection method, sol gel method, laser irradiation method, co-sputtering method and ion exchange method [16,17]. The ion-exchange method combined with an atmospheric post-heat treatment is a simple and effective preparation method. Metal ions are incorporated into the glass host materials through a simple ion exchange method and later the metal ions are reduced to metal atoms by controlling the post-heat treatment process conditions. The current work shows that the SPR absorption of glass doped with metal NCs vary with size, concentration, microstructure, shape and interface structure of the clusters [16,17]. The plasmonic properties are significantly controlled by changing the size of the metal NCs. It is worth noting that the copper nanoclusters diffused in ion exchanged glass is of great advantage for the third order nonlinear optical features and blue-green luminescence properties of the Cu^+ ions with the possible application in the field of laser technology and all-optical switching devices [18]. Generally, Cu exists in the soda-lime glass matrix in different oxidation state such as Cu^0, Cu^+, Cu^{2+} and forms either Cu^0 or Cu_2O nanoclusters in glass matrix which gives rise to the distinctive optical features in photonics devices [18]. The spectroscopic features of Cu nanoclusters in the glass can be related to its structural and electronic configurations. It is therefore essential to study structural as well as electronic configuration and understand the formation of different oxidation states of Cu in an ion exchanged soda-lime glass matrix.

The NLO parameters such as third order NLO susceptibility, nonlinear absorption and nonlinear refraction of glass doped with Cu NCs were investigated by the femtosecond Z-scan technique. The glass materials doped with Cu NCs exhibited a switching behavior (SA in RSA). The embedded Cu NCs in the glass host materials annealed at different temperatures demonstrated fascinating step wise behavior such as pure SA, switching (SA-RSA)

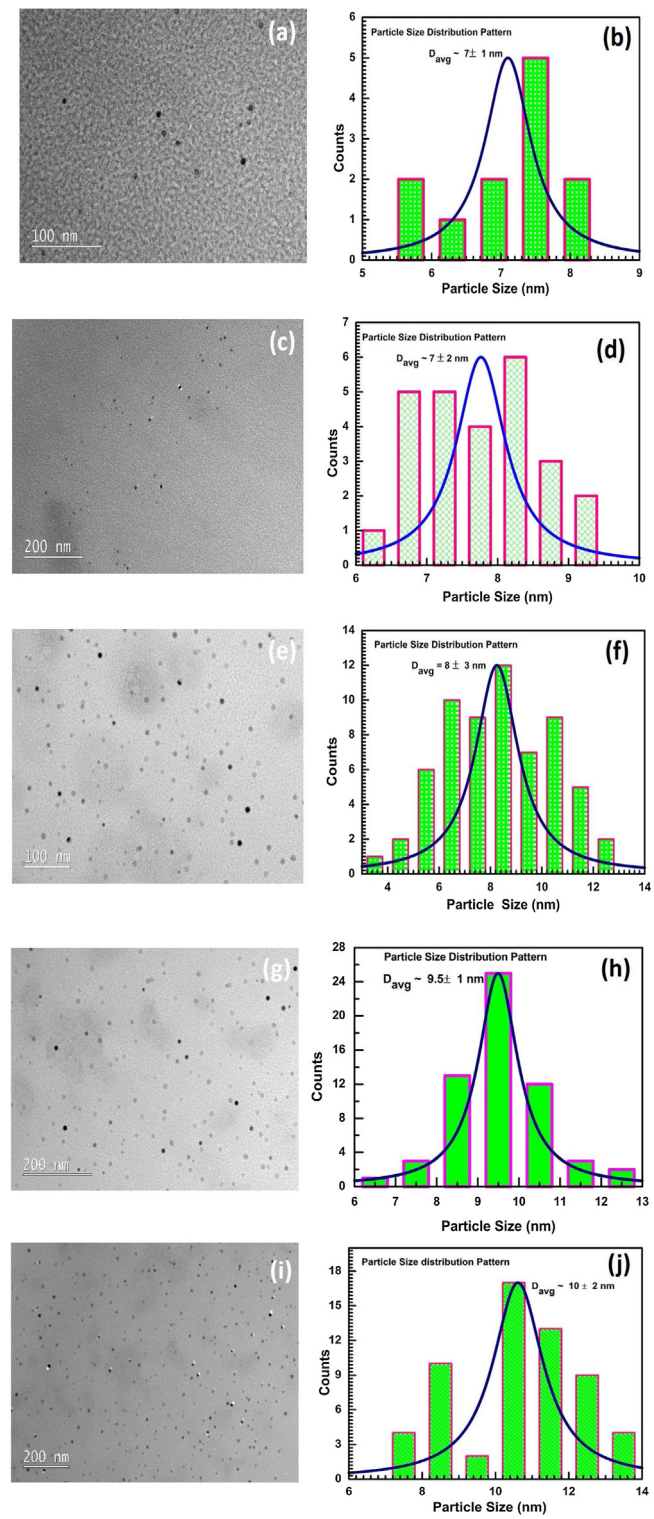

Fig. 2. (a) TEM images and particle size distribution curves: (a, b) 450 °C; (c, d) 500 °C (e, f) 550 °C; (g, h) 600 °C; (i, j) 650 °C.

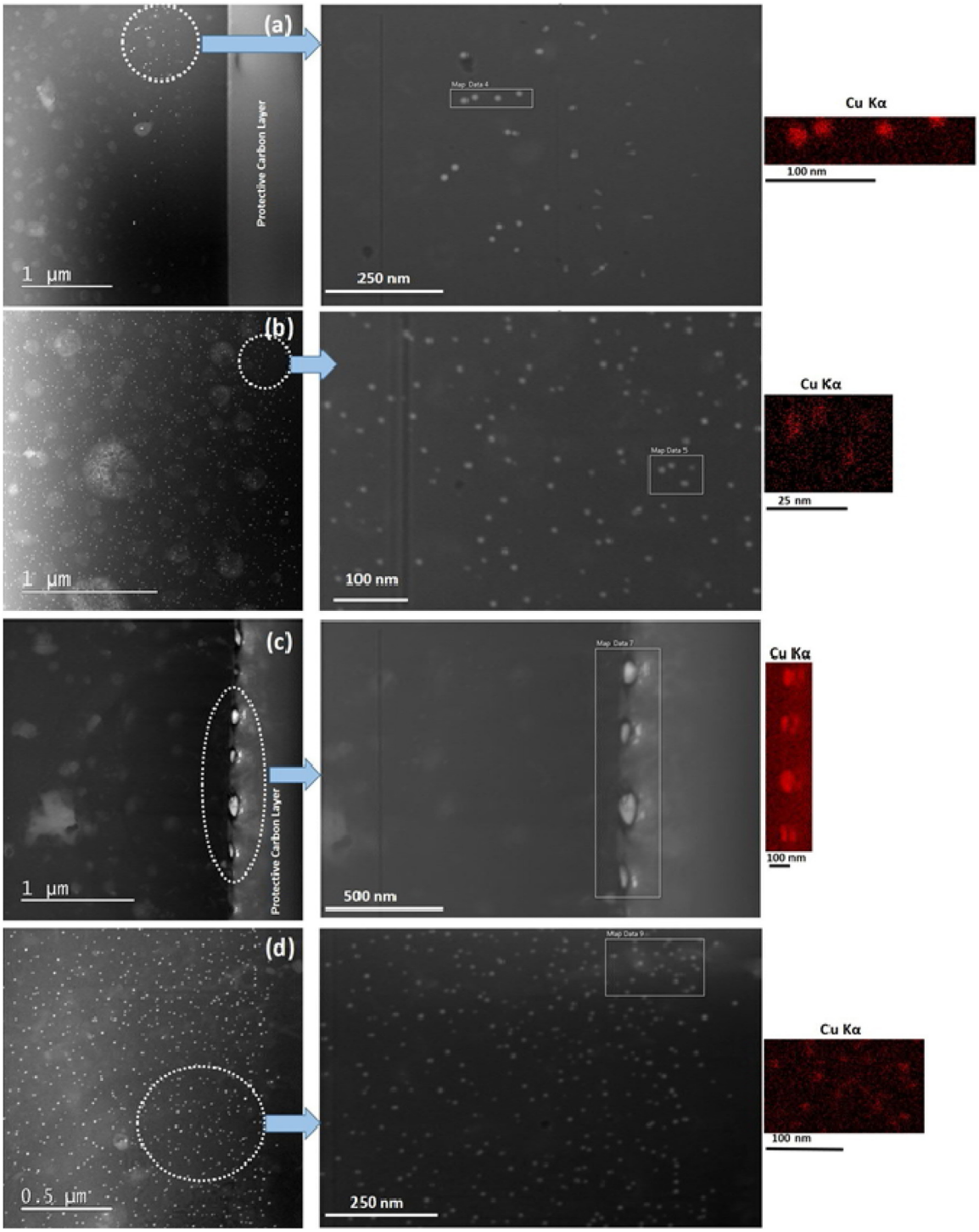

Fig. 3. HAADF-STEM images: for (a) 500 °C; (b) 550 °C; (c) 600 °C; (d) 650 °C, as well as the EDS Cu images.

and pure RSA with increasing annealing temperature. In this work, a study of nonlinear refraction of glass doped with Cu NCs before and after atmospheric post heat-treatment is also presented.

2. Experimental details

The ion-exchange method combined with atmospheric heat treatment is a simple and effective method to produce spherical Cu NCs in glass materials. Commercial glass slides (76 mm × 26 mm × 1 mm) with a transition point temperature of 650 °C were considered the best choice as a host matrix for the formation of Cu NCs. The chemical composition of the glass was 72.0% SiO_2, 14.0% Na_2O, 0.6% K_2O, 7.1% CaO, 4.0% MgO, 1.9% Al_2O_3, 0.1% Fe_2O_3, 0.3% SO_3 (calculated based on weight %). These glass slides were cleaned before the ion exchange experiment with different solvents such as water and trichloroethylene to remove the surface impurities. A glass slide was covered by the mixed salt of $CuSO_4{\cdot}5H_2O$: Na_2SO_4 (54:46 mol%) powder in an alumina crucible.

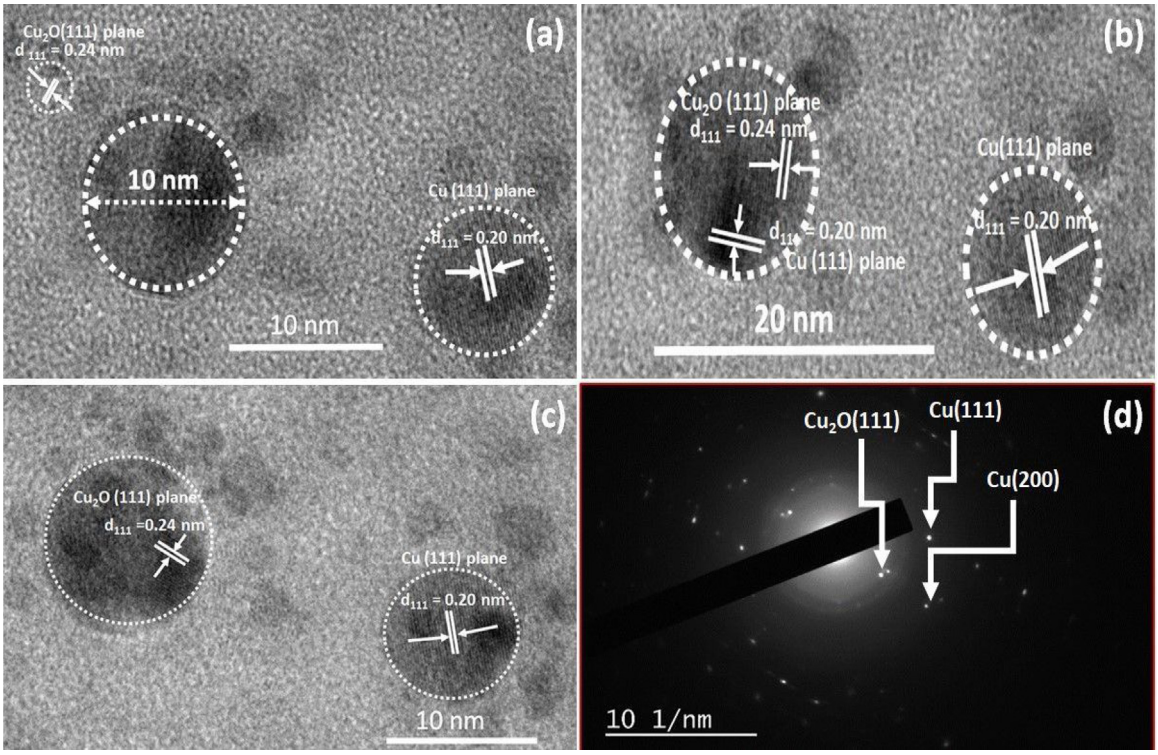

Fig. 4. HRTEM images for: (a) 550 °C; (b) 600 °C; (c) 650 °C; and (d) SAED pattern at 650 °C.

This was heated up to 590 °C where the temperature was kept for 2 min (different from a previous experiment of ours where a much longer time of 15 min was used and a thermodynamic study on the nucleation and growth of a much higher concentration of Cu in the glass matrix was studied [18]). The furnace was allowed to cool after which the glass slide was removed from the salt and washed with different solvents such as water and trichloroethylene to remove the impurities on the surface. These samples were then placed in a tube furnace containing atmospheric gas at 450, 500, 550, 600 and 650 °C for 1 h, after which they were allowed to cool. In this work, the nucleation and growth of the Cu NCs were controlled by the post-heat treatment. The Cu ions were incorporated into the glass host and the Cu ions were subsequently converted into Cu atoms. The SPR absorption of the Cu doped glass samples was recorded by using a dual beam UV–visible spectrophotometer (HITACHI U 3300 model) in the wavelength range of 300–800 nm. The intensity of the SPR absorption of the Cu NCs increased rapidly after the post-heat treatment process due to the growing spherical Cu NCs distributed homogeneously in the glass.

The diffusion of Cu in the glass substrate before and after heat treatment was investigated by Rutherford backscattering spectrometry (RBS). RBS analysis was performed using He^+ ions with energy of 1.6 MeV at a backscattering angle of 165°. The beam current maintained at about 10 nA and charge of 8 μC was collected during the measurements.

The photoluminescence (PL) properties of glass doped with Cu NCs were measured using a FS5 spectrofluorometer from Edinburgh Instruments. The PL data of glass doped with Cu NCs were measured when excited by two different wavelengths i.e. 280 nm and 325 nm, respectively.

The structure, morphology and size of the Cu NCs were studied by X-ray diffraction (XRD) and transmission electron microscopy (TEM). It is essential to optimize the post heat treatment process for the growth of the spherical shaped Cu NCs distributed uniformly in the glass. A D8-Advance X-ray diffractometer (Bruker, Germany, $\lambda = 0.15408$ nm, acceleration voltage 40 kV, scanning rate: 0.02°/s, 2θ scanning range: 10°–90°) was used for the structural analyses. The morphology and size of the Cu NCs were obtained using a JEM-2100 TEM operated at 200 kV. Energy dispersive X-ray spectroscopy (EDS) was used for elemental mapping and chemical composition analysis using an Oxford XMax 80 detector. Image J software was used to calculate the size of the spherical shaped Cu NCs formed in the glass matrix.

X-ray photoelectron spectroscopy (XPS) (PHI 5400 spectrometer) was used to study the chemical state of the Cu doped glass samples after annealing. The full detail of XPS setup can be found in Ref. [19]. The NLO of the Cu NCs was analyzed by using a femtosecond laser Z-scan technique at the wavelength of 800 nm to understand the behavior of the nonlinear absorption and nonlinear refraction traces, respectively. The Z-scan experimental details are reported in our earlier works [20–23]. The input beam (diameter ~2 mm) was focused using a 100-mm focal length convex lens while the sample was placed on a 1-μm resolution translation stage and the scanned transmission data was manually entered by using the detector for each Z position. The laser peak intensity has been controlled to be <1 GW/cm^2 to avoid damage of the sample using neutral density filters. The value of change in phase $\Delta\Phi$ was ensured to be less than π [24]. The nonlinear absorption and nonlinear refraction coefficients were acquired by fitting Z-scan curves via solving a set of differential equations numerically for the sample transmittance.

3. Results and discussion

3.1. Plasmonic properties of Cu NCs–UV–Vis

The optical absorption spectra of the pristine sample and the annealed samples are shown in Fig. 1. The pristine sample shows a broader SPR absorption peak at 568 nm, which is a characteristic of Localized Surface Plasmon Resonance (LSPR) of the Cu NCs formed during the ion exchange process [18,25,26]. A blue shift of 8 nm of the SPR absorption peak was observed from 568 nm to 561 nm after

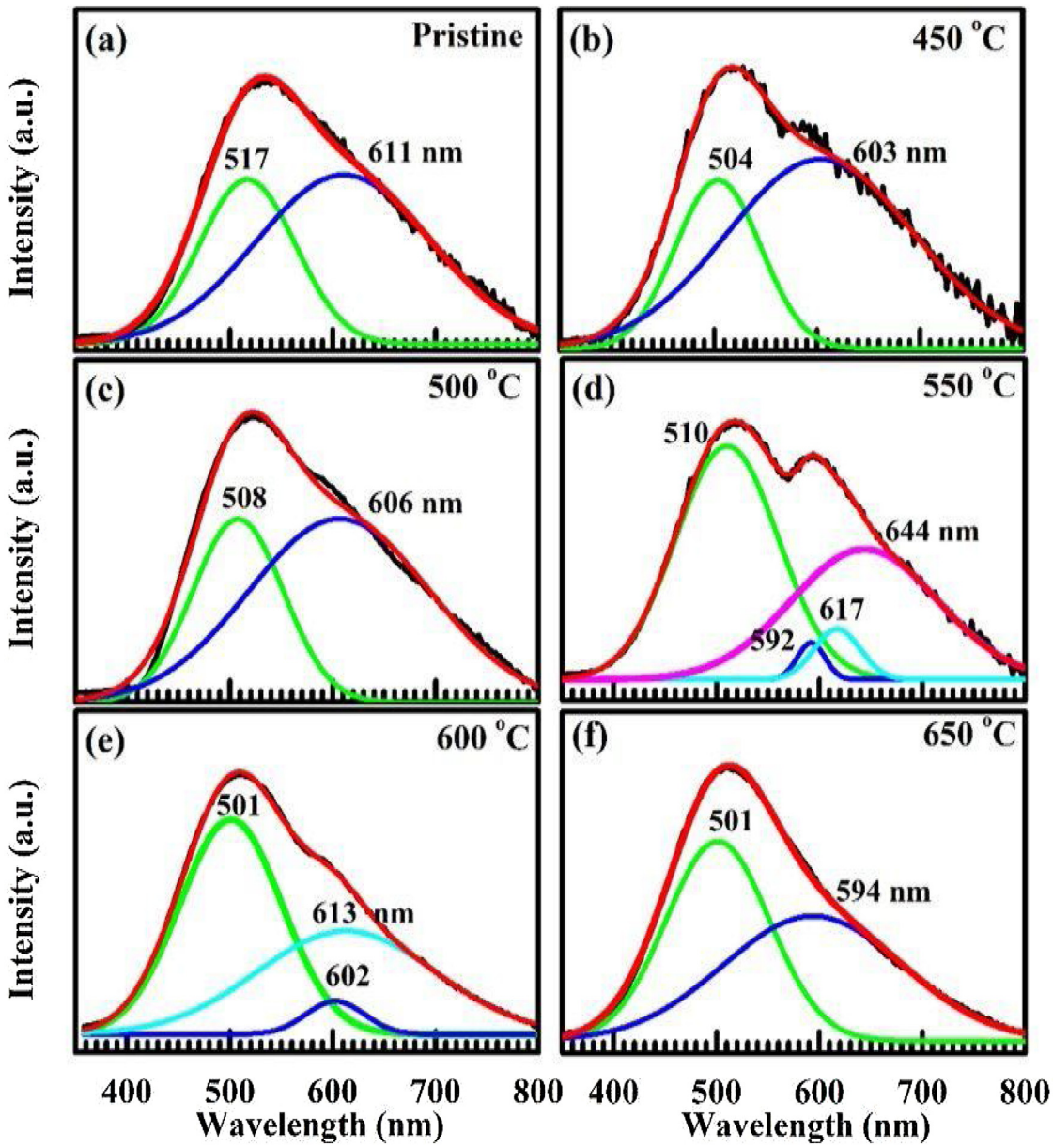

Fig. 5. PL spectra excited at 280 nm of the pristine sample and after annealed at various temperatures from 450 °C up to 650 °C.

the post heat treatment process as shown in Table 1 of the electronic supplementary materials [ESM-1].

This kind of a small blue shift of the plasmonic peaks indicates that the refractive index property of the host or the size of the Cu NCs is thermal heat treatment-dependent.

In the optical absorption spectra, the LSPR peak intensity increased with the atmospheric post heat-treatment, which is assigned to temperature induced Cu NCs growth as $Cu^{2+}/Cu^{+} \rightarrow Cu^{0}$. The refractive index decreased at the metal-dielectric (glass) interface with the post heat treatment conditions [26,27]. The blue shift is assigned due to the depletion of the effective refractive index at the metal-dielectric (glass) interface.

The FWHM of the LSPR absorption peak was found to decrease with the post heat-treatment process. The shifting of the plasmonic peaks was observed due to the change in the cluster sizes during thermal treatment. In an earlier studies, Manikandan et al. [28] also observed a similar kind of change in the SPR peaks, which was attributed due to the spill out of the conduction electrons, resulting in the electron density drop thus effecting the change in SPR peaks. The higher intensity of the plasmonic peak suggested a higher volume fraction of Cu nanoclusters embedded in the glass matrix. The FWHM of the LSPR absorption peak was found to decrease with the post heat-treatment process. In an earlier study a similar kind of reduction in FWHM of the SPR absorption peak with increasing the cluster size was observed, which was also observed for small NCs (less than 10 nm) due to the mean free path of the electrons [18,25,29].

The average size of the Cu NCs was calculated using the following equation [18,25].

$$d = 2R = 2\hbar V_f / \Delta E_{1/2} \quad (1)$$

where d = average size of particle, $\hbar$ = Planck's constant, V_f = Fermi velocity in bulk Cu (1.57×10^6 m/s) and $\Delta E_{1/2}$ is the FWHM of LSPR absorption peak. These results were closely matched with the Cu NC size which was smaller than the mean free path of the electron (39 nm at RT) for bulk Cu [26,30]. The average size of the Cu NCs was estimated to be 6.2, 6.6, 7.1, 7.9, 8.6 and 9.8 nm for the pristine, 450, 500, 550, 600 and 650 °C samples, respectively.

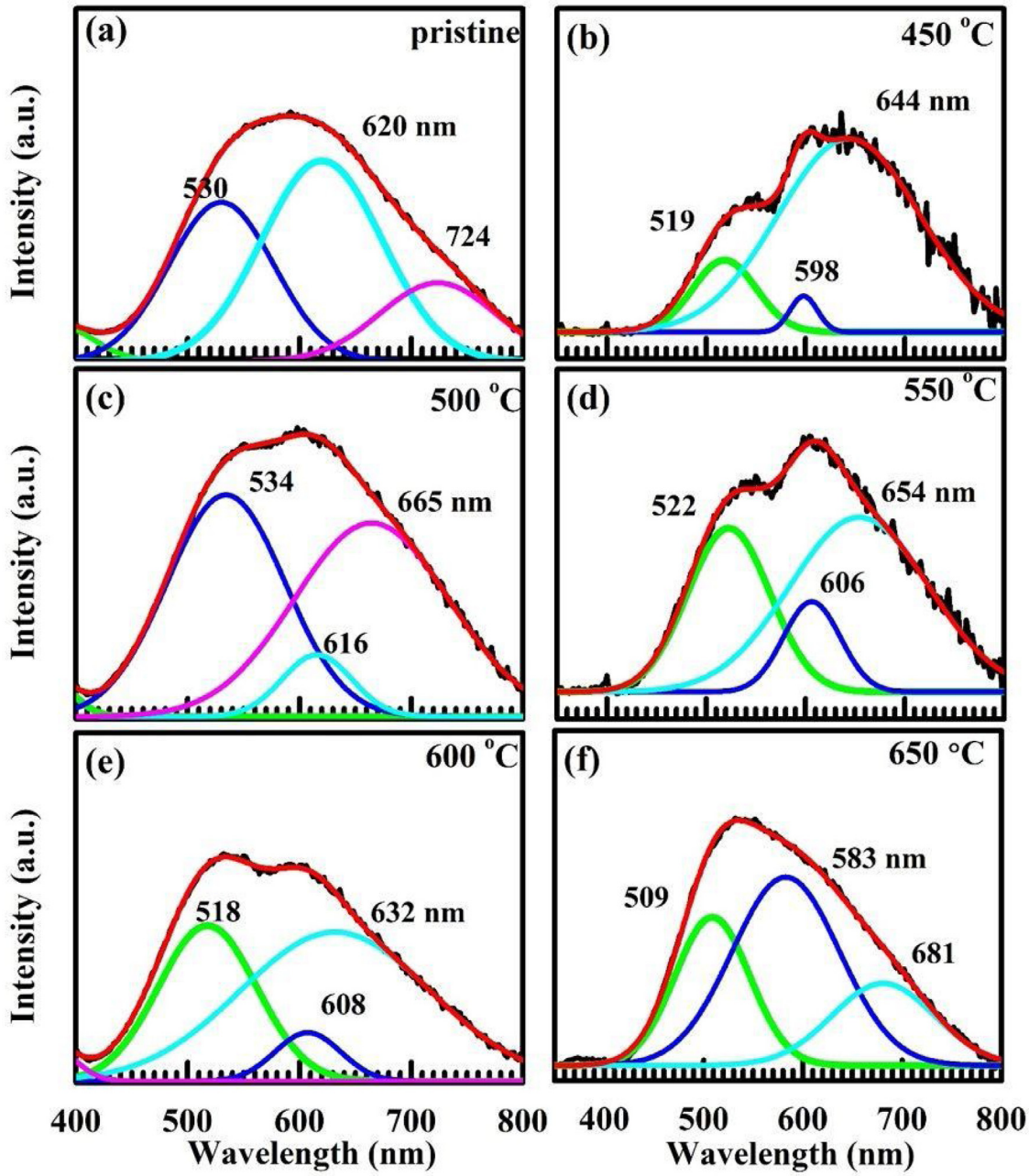

Fig. 6. PL spectra excited at 325 nm of the pristine sample and after annealed at various temperatures from 450 °C up to 650 °C.

SPR peak position and width as well as NCs size for different post heat treatment temperatures are shown in Table 1 of the electronic supplementary materials [ESM-1].

3.2. Morphological studies – TEM analysis by means of FIB-SEM

The particle size and microstructure of Cu doped glass samples were analyzed by TEM. Fig. 2 shows TEM images of the samples annealed at various temperatures. Cu NCs were introduced in the glass with regular spherical geometries with a particle size distribution between 7 and 10.2 nm depending on the annealed temperature. The sizes of these NCs were calculated using the histogram distribution curves.

Fig. 3 shows the high angle annular dark field scanning transmission electron microscopy (HAADF-STEM) images of the samples annealed at various temperatures (i.e. 500–650 °C). The images reveal that the Cu NCs consisted of small clusters distributed in the glass matrix. These NCs showed a good dispersion and no agglomeration occurred (Fig. 2), which was further confirmed by the corresponding EDS mapping analysis. The EDS mapping confirmed that the small, bright particles consisted of Cu NCs (red spots in Cu EDS) that formed in the glass matrix. Some of the large bright Cu NCs were also observed in the surface region of the glass matrix and were confirmed by EDS analyses as shown in Fig. 3(c). (Please note the changes in the scales that were used on all the HAADF-STEM and EDS images.) The diffusion of Cu atoms near the surface region of the glass matrix was discussed using RBS studies as shown in electronic supplementary materials [ESM-2].

Fig. 4(a)–(c) shows HRTEM images of the samples annealed at 550, 600 and 650 °C, respectively. The HRTEM images indicated that the spherical Cu NCs consisted of crystals with interplanar spacings of 2.0 nm and 2.4 nm, which correspond to the (111) plane of

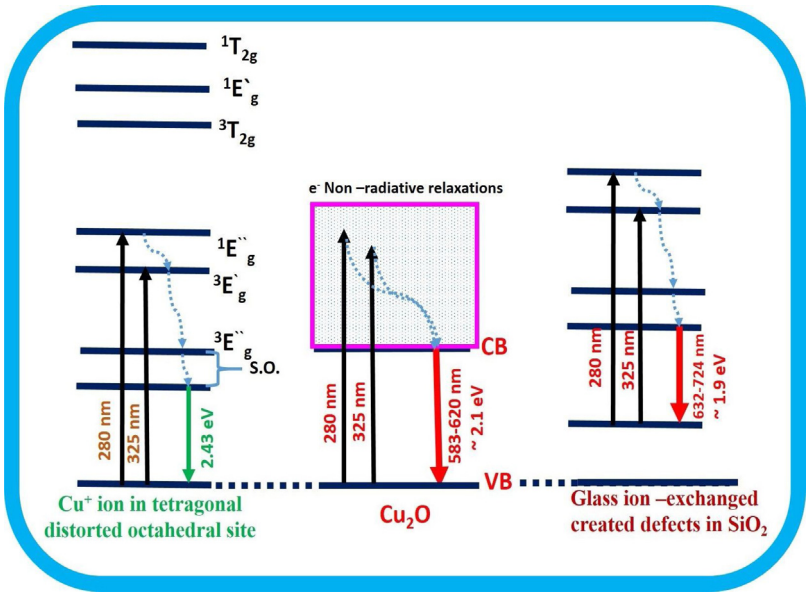

Fig. 7. Schematic energy level diagram of the Cu NCs embedded in the glass. The energy levels of the Cu^+ ions are adapted from Ref. [31] (S.O. denotes spin-orbit split components), while the energy levels of the defect in SiO_2 is taken from Ref. [32].

pure Cu metal (PDF no. 04-0836, 2.0 nm for (111) plane) and Cu_2O (PDF no. 34-1354, 2.4 nm for (111) plane). The diffraction pattern spots corresponding to Cu_2O (111), Cu (111) and Cu (200) diffraction planes are shown in Fig. 4(d). These results are closely matched with XRD based results as discussed in electronic supplementary materials [ESM-3].

According to XRD, TEM and EDS analyses, it may be concluded without doubt that Cu NCs with regular geometries formed in the soda-lime glass matrix.

3.3. Optical properties of Cu NCs–PL

Two different excitation wavelengths of 280 and 325 nm have been used to explore the defects associated with the exchange of Cu ions into the glass matrix as shown in Figs. 5 and 6. The glass used without ion exchange only shows a weak emission in the infrared region (~750 nm) as shown in electronic supplementary materials [ESM-4], different to what is observed for the ion-exchanged samples. Therefore the PL mainly originates due to the Cu incorporation and its consequences for the charge imbalances of the network modifiers (such as Na, Si, O etc.) in the silica matrix of glass substrate. Luminescence peaks may originate from the electron transitions between energy levels of the Cu^+ $3d^94s^1$ and $3d^{10}$ states. Debnath[31] studied the site-dependent luminescence of Cu^+ ions in silica glass, reporting that emission occurred near 417–433 nm for Cu^+ ions in sites of cubic symmetry and near 490 nm in sites of tetragonal-distorted octahedral symmetry. In the present results, no PL emission was observed in the range of 400–450 nm (Figs. 5 and 6) suggesting that the Cu^+ ions were not located at cubic sites of Cu^+ ion-exchanged glass matrix.

The Laporte rule does not allow the electronic transition between $3d^94s^1$ and $3d^{10}$ for free Cu^+ ions [32–34], but when Cu^+ and O in the glass form a distorted octahedral coordination, the asymmetry of local electric field around Cu^+ ions thereby allows this forbidden electronic transition. The emissions in the range of 501–534 nm for Figs. 5 and 6, being fairly close to the wavelength of 490 nm given by Debnath [31], are therefore assigned to Cu^+ ions in tetragonally distorted octahedral sites. The difference in wavelength as well as variations between the samples may be due to differences in the host material and defects in the glass.

In addition to these, PL bands in the range 583–620 nm and 632–724 nm were observed. The semiconductor Cu_2O, shown to be present in the glass using XRD and TEM, has a band gap of 2.1 eV (~590 nm) [35] and may account for the first of these PL bands. The PL band in the range of 583–620 nm has been observed in the different samples whose origin is not clear yet, but is believed to be as a result of defects associated with copper oxides in the glass matrix [35].

The second band is attributed to defects associated with silicon dioxide having an emission energy reported as 1.9 eV (653 nm) [32–34].

Fig. 7 shows the PL energy level diagram of glass doped with Cu NCs. Excitation at 280 or 325 nm may excited the Cu^+ ions, the Cu_2O NCs or defects in the glass host independently, producing the different emission bands observed. In the ion-exchange process the exchange of ions and aggregation will form defects. Annealing and the conversion of Cu ions to neutral atoms which diffuse creates further defects. This results in multiple emission bands (632–724 nm) in different samples at different annealing temperatures. The peak positions of the PL emission as excited by the two wavelengths of 280 and 325 nm are shown in Table 2 of the electronic supplementary materials [ESM-5].

3.4. Bonding of Cu NCs – Raman

Fig. 8 presents Raman spectra of the Cu pristine sample and post heat treatment samples. The Raman bands for the pristine sample were observed at 290, 560, 670, 783, 960 and 1084 cm^{-1}. The Raman band at 290 cm^{-1} was assigned to the Cu_2O [36]. A red shift of the Raman band was observed after the post heat-treatment as shown in Fig. 8(a)–(c). Cu^+ exists in the glass matrix and was assigned to the Raman band in the range of 250–300 cm^{-1}, 580–630 and 1080 cm^{-1} and weak features were also observed in the Raman spectrum of the region [35]. The vibration observed at 573 cm^{-1} was assigned to bending vibrations within inter-tetrahedral bonding, and the others between 900 and 1300 cm^{-1} were assigned to Si–O stretching vibrations of the silica tetrahedral (in our case observed at 1084, 1087, 1106 cm^{-1}) [36,37]. It has been also reported that the Raman spectra corresponding to glass doped with Cu NCs shows a strong Raman peak intensity at 500 cm^{-1} band due to the Si–O bending and the band between 750

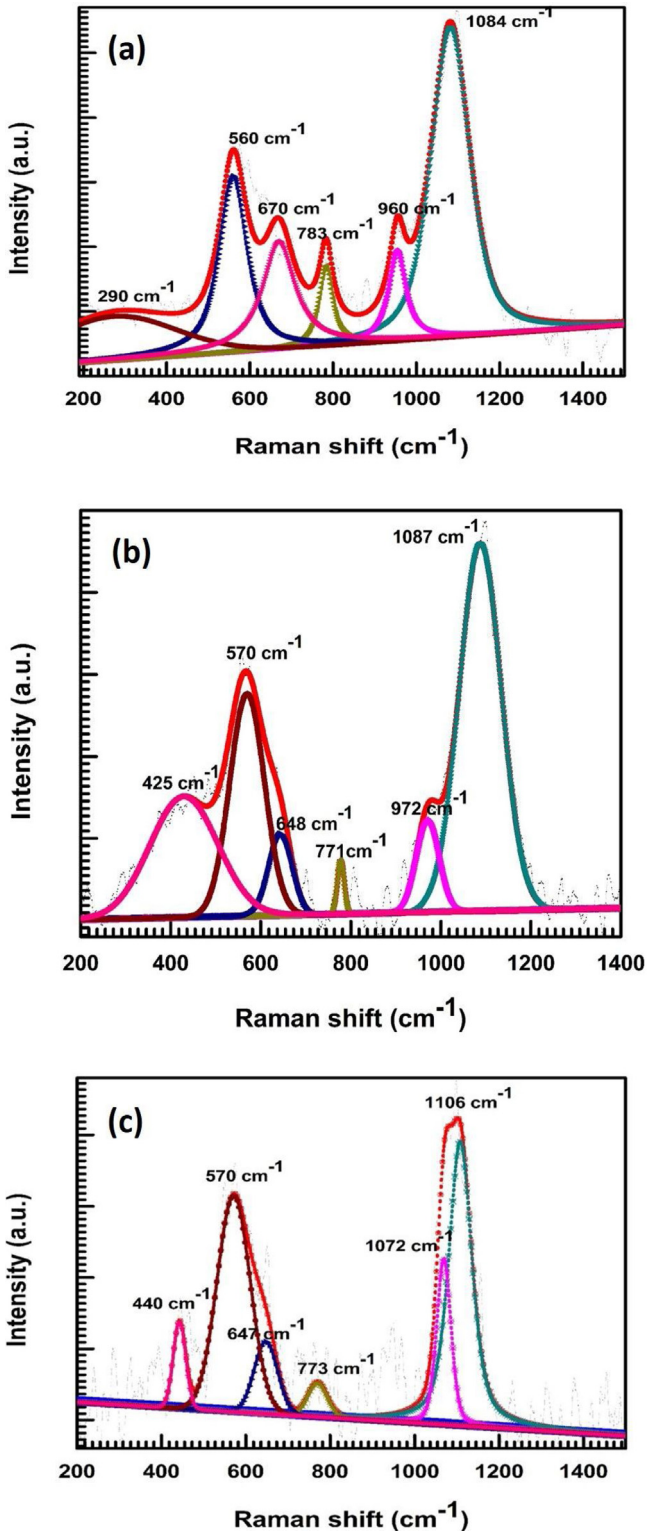

Fig. 8. Raman spectra of the glass doped with Cu NCs; (a) pristine sample; annealed at (b) 600 °C for 1 h; (c) 650 °C for 1 h.

to 1150 cm^{-1} indicates the Si–O stretching components, as earlier observed for the Cu atoms in a glass matrix. But in our case the vibration region of the thermally treated Cu pristine sample occurred at 566 cm^{-1} which assigned to Si–O bending and Si–O stretching band appeared at 1098 cm^{-1} observed for the Cu atoms formed near the glass surface. The intensity ratio corresponding to Si–O bending and stretching components both exhibited crystalline as well as amorphous behavior with the higher degree of the polymerization index [38]. It was earlier reported that Raman bands for Cu_2O are observed at ~220 and 280–300, 345 cm^{-1} and the Raman band observed at 625 cm^{-1} indicated that Cu atoms formed in the glass material [36].

In our case, an intense peaks lies below 400 cm^{-1} which may be related to the signature of the Cu_2O in the glass matrix as also discussed in XRD and XPS results. Raman signature of Cu^0 atoms was observed for the pristine sample at 670 cm^{-1} and 648, 647 cm^{-1} for the heat treated Cu sample at 600 °C and 650 °C.

3.5. Chemical properties of Cu NSs–XPS

The XPS survey spectrum (Fig. 9(a)) of the pristine sample shows the expected elements such as C, O, Cu, Si, Na and Ca. The C 1s peak for the pristine sample was deconvoluted to C–C, metal carbide, C–OH, C–O–C, C=O and C≅O contributions as shown in Fig. 9(b). Fig. 9(c) shows the energy region of the O 1s level for the pristine sample. The fits revealed H_2O, Cu_2O, CO, OH or defects and CO_3 contributions as indicated. The XPS spectrum of the Cu pristine sample corresponding to the Cu 2p region was decomposed using Gaussian–Lorentzian curve fitting. According to the fits, the binding energies were 932.3 eV for the Cu_2O and 932.8 eV for Cu^0 neutral atoms, 934.2 eV assigned to $CuCO_3$, respectively (Fig. 9(d) which confirmed the presence of neutral Cu atoms [18,39]. It is well known that the binding energies corresponding to Cu^0 neutral atom and Cu_2O are very close [18]. So we conclude that both pure Cu^0 and Cu_2O phases exist in the pristine sample.

The XPS spectra of the samples annealed at 500–650 °C are shown in Fig. 9(e)–(h). The binding energies of the Cu $2p_{3/2}$ of the sample annealed at 500 °C (Fig. 9(e)) were located at 932.8 eV for Cu^0 or Cu_2O, 934.2 for $CuCO_3$ and 935.7 eV for $CuCl_2$. $CuCl_2$ is also observed because the samples were cleaned with different solvent such as water, ethanol and trichloroethylene.

Similar results have been observed for the sample annealed at 550 °C as shown in Fig. 9(f). The binding energy corresponding to Cu 2p for the samples heated at 600 °C and 650 °C are located at 932.3, 932.8 eV for Cu^0 or Cu_2O and 932.4 for Cu or Cu_2O, 934.1 eV for $CuCO_3$, 935.6 for $CuCl_2$ as shown in Fig. 9(g)–(h). The XPS peak intensity of the Cu 2p spectrum in the pristine sample was observed as a more intense peak compared to the heat-treatment samples. It means a higher population of the Cu atoms in the pristine sample formed on the glass surface. But after heat-treatment, the Cu atoms were uniformly distributed in the glass and the XPS peak intensity reduced slightly, which confirmed the diffusion of Cu atoms in the glass material. The XPS results confirmed that the chemical state of Cu in the glass materials was in the form of both Cu^0 and Cu_2O. Post thermal treatment in air atmosphere leads to the diffusion of oxygen atoms also into the near-surface of Cu-doped layer in the soda lime glass, which shows the oxidation of Cu in the form of Cu, Cu_2O nanoparticles on the surface of the glass matrix.

3.6. Nonlinear optical properties of Cu NCs–Z-scan

Saturable absorption is obtained for glass doped with Cu NCs. As observed in Fig. 10(a), the output transmittance increased as the sample reached the focal point and obtained maximum transmittance at the focal point. To interpret SA, it is necessary to evaluate the saturation intensity (I_S) coefficient yielding the absorption coefficient as [40].

$$\alpha(I) = \alpha_0 \frac{1}{1+\frac{I}{I_s}}, \ldots I = \frac{I_{00}}{1+\left(\frac{z}{z_0}\right)^2} \quad (2)$$

where I_{00} = laser peak intensity, I_S = saturation intensity, z_0 = Raleigh range, α_0 = linear absorption coefficient and z refers

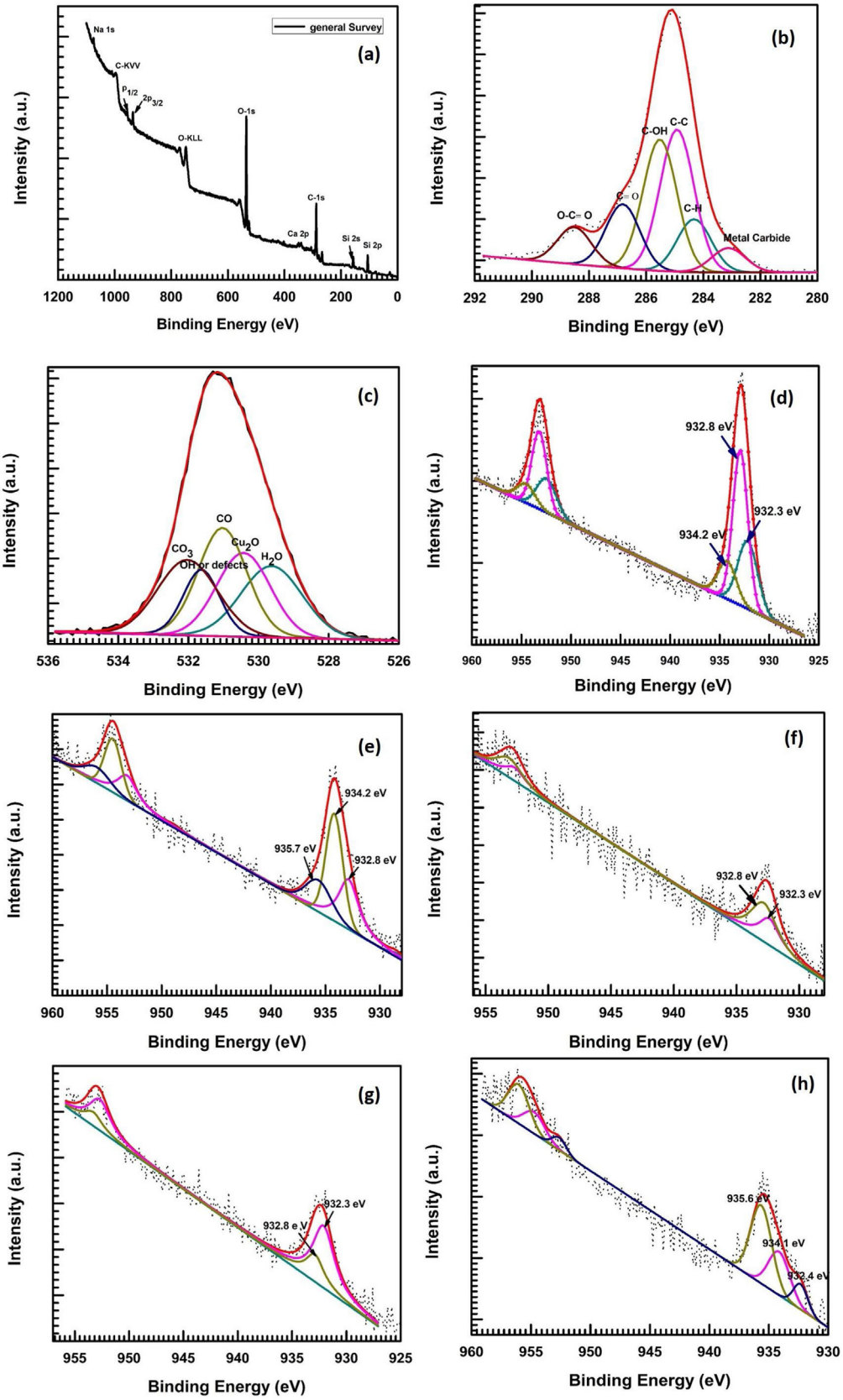

Fig. 9. XPS spectra of the Cu region: (a) survey scan (Pristine); (b) C 1s (Pristine); (c) O 1s (Pristine); (d) Cu 2p (Pristine); (e) Cu 2p for 500 °C; (f) Cu 2p for 550 °C; (g) Cu 2p for 600 °C and (d) Cu 2p for 650 °C.

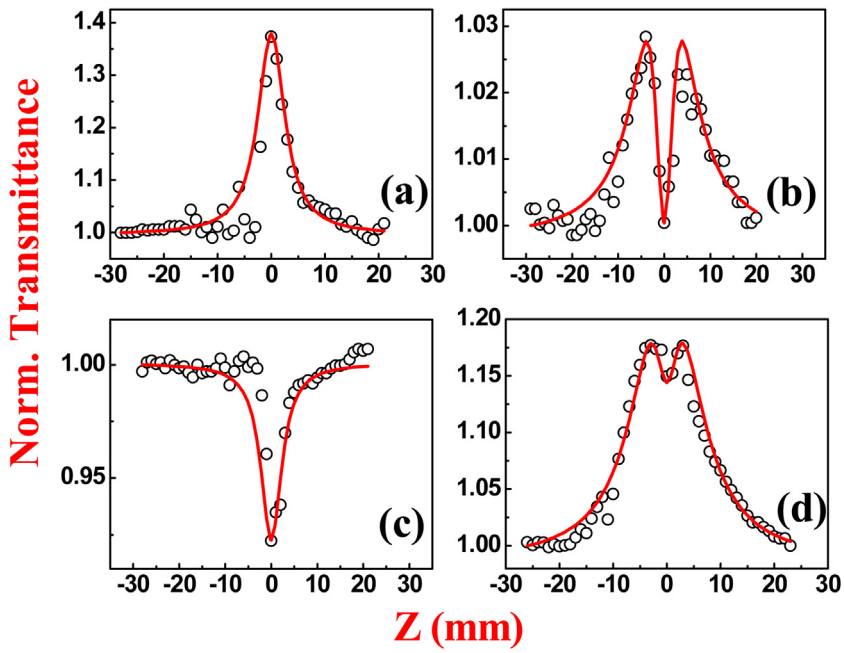

Fig. 10. Open aperture Z-scan data of (a) Cu NPs without annealing, (b) Cu NPs-550 °C, (c) Cu NPs-600 °C and (d) Cu NPs-650 °C were recorded at 142 MW/cm^2 with 800 nm wavelength by ~150 fs pulses.

to the laser beam propagation direction. As for purely nonlinear absorption, the nonlinear transmittance is collected beside the *z*-axis propagating through the glass doped Cu NCs expressed by [24].

$$\frac{dI}{dZ*} = -\alpha(I)I \tag{3}$$

To acquire the theoretical open aperture Z-scan curve, it is requisite to evaluate Eq. (3) at every point of Z along the sample likewise the I(z) changes with z point. This model was used to fit the data in Fig. 11(a) and to obtain the I_S = 135 MW/cm^2 value at an input peak intensity of 142 MW/cm^2. The dispersed Cu NCs demonstrated lower saturation intensity than the input peak intensity due to efficient bleach in the ground state by surface plasmon resonance. A similar SA behavior was demonstrated by Wang et al. [41] for an array of gold nanoparticles due to plasmon band absorption at a high peak intensity. It could be observed that the SA behavior will slowly die out when the increment takes place in the size of plasmonic nanoparticles. Fig. 10(b) illustrates a nonlinear absorption trace recorded at a peak intensity of 142 MW/cm^2 for the embedded Cu NCs in soda-lime glass annealed at 550 °C (Cu NCs-550 °C). It is noted that the nonlinear transmittance appeared as a peak at lower irradiance. However, a minimum transmittance was exhibited at higher irradiance (focal point) and was pointing toward a switching behavior from SA to RSA (m-shape). To explain the switching behavior from SA to RSA, the saturable absorption coefficient (α_0) and two photon absorption (TPA, β) coefficients were added, which generate the total absorption coefficient [42,43] as.

$$\alpha(I) = \alpha_0 \frac{1}{1 + \frac{I}{I_s}} + \beta I \tag{4}$$

where the first term presents the negative nonlinear absorption and the second term presents positive nonlinear absorption such as RSA and/or TPA. These coefficients were evaluated by fitting the M shaped curve using Eq. (4) along with Eq. (3) and the values of coefficients are I_S = 72 MW/cm^2 and effective two photon absorption coefficient (β) = 20 cm/GW. The Cu NCs-550 °C showed a lower I_S than the Cu NCs value which could be due to strong ground state plasmon absorption. The observed dip in the m-shape represents two photon absorption which could be possibly due to excited state absorption [42]. This behavior is dissimilar from pure RSA (TPA) and RSA–SA (W-behavior). The m-shaped trace in the Z-scan transmittance changed to pure RSA (Fig. 10c) as the dimensions of the Cu NCs increased from 14.6 nm to 17 nm. Fig. 10c illustrates a pure RSA trace for embedded Cu NCs in soda-lime glass annealed at 600 °C (Cu NCs-600 °C), recorded at an input peak irradiance around 142 MW/cm^2. The obtained β = 40 cm/GW for Cu NCs-600 °C is larger than in the case of Cu NPs-550 °C due to the strong dip exhibited in the trace of the Z-scan transmittance for Cu NCs-600 °C which is motivated by three different mechanisms. The first term described the transition of electron started from ground state to the higher excited state by the coincident of two photon absorption [44]. The second term i.e. the excited state absorption (ESA) indicates two-step two photon absorption [43]. Third, free carrier absorption related to nonlinear scattering effect [37]. Interestingly, the embedded Cu NCs annealed at 650 °C (~16 nm) exhibited M-shaped curve at an input peak irradiance of 142 MW/cm^2, as shown in Fig. 10(d) and obtained saturation intensity (I_s = 33 MW/cm^2) and effective two photon absorption coefficient (β = 16 cm/GW) by fitting this M-shaped curve using the above mentioned model Eqs. (2) and (3). The similar kind of behaviors was studied in Au nanoparticle array [43], Cu nanoparticles in solutions [19] and semiconductor nanoparticles [45].

The closed aperture Z-scan method was studied to find the sign and magnitude of the nonlinear refractive index of the glass doped with Cu NCs. Fig. 11 showed the closed aperture curves of dispersed/embedded Cu NCs in the soda-lime glass host (a) Cu NCs, (b) Cu NCs-550 °C, (c) Cu NCs-600 °C and (d) Cu NCs-650 °C, recorded at an input irradiance of 27 MW/cm^2. In these traces, the peak- valley phase of the Cu NCs (Cu NCs, Cu NCs-550 °C and Cu NCs-650 °C) exhibited a traditional self-focusing behavior, representing the sign of the real part of $\chi^{(3)}$ (n_2) as positive. The sample Cu NCs-600 demonstrated self-defocussing curve implying the sign of the real part of $\chi^{(3)}$ (n_2) as negative. The reason behind the positive and negative nonlinear refractive index could be due to ground state plasmon absorption and free carrier absorption, respectively. The refractive index values of all samples were found to be 2×10^{-11} cm^2/W, 0.5×10^{-11} cm^2/W, 0.6×10^{-11} cm^2/W and

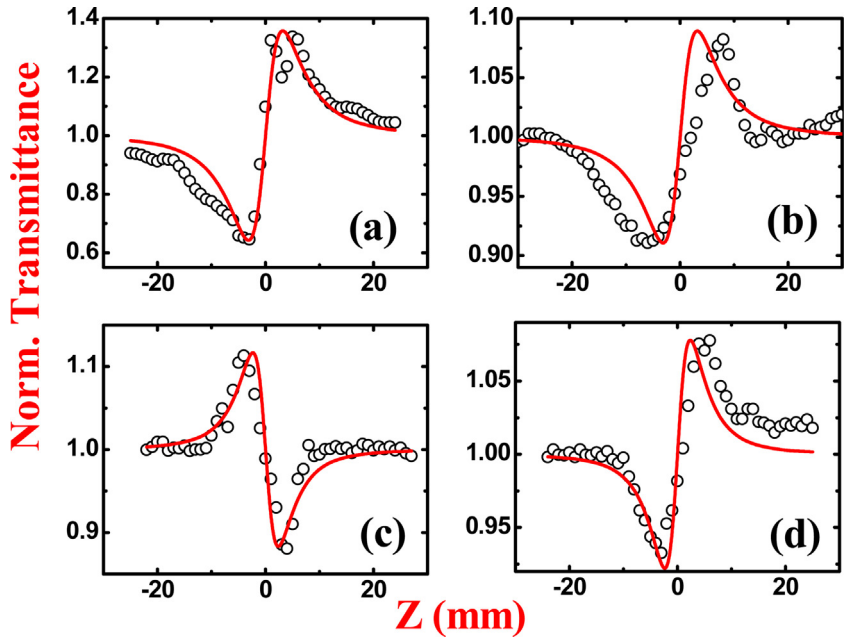

Fig. 11. Closed aperture Z-scan data of (a) Cu NPs without annealing, (b) Cu NPs-550 °C, (c) Cu NPs-600 °C and (d) Cu NPs-650 °C were recorded at 27 MW/cm^2 with a 800 nm wavelength by ~150 fs pulses.

0.5×10^{-11} cm^2/W for Cu NPs, Cu NPs-550, Cu NPs-600 and Cu NPs-650, respectively, according to the following CA Z-scan transmittance [46–48].

$$T\left(\frac{z}{z_0}\right) = 1 - \frac{4\left(\frac{z}{z_0}\right)\Delta\phi_0}{\left[\left(\frac{z}{z_0}\right)^2 + 1\right]\left[\left(\frac{z}{z_0}\right)^2 + 9\right]} \quad (5)$$

where Z represents sample position; $z_0 = \pi\omega_0^2/\lambda Z_0 = \frac{\pi\omega_0^2}{\lambda}$ i.e. the Rayleigh range; ω_0 = beam waist at the focal point (Z = 0); λ = wavelength; $\Delta\phi_0$ indicates nonlinear phase shift. Nonlinear refractive index can be calculated from $\Delta\phi_0$.

$$\Delta\phi_0 = \frac{\Delta T_{p-v}}{0.406(1-S)^{0.25}} \quad (6)$$

where S (25%) indicates aperture linear transmittance and is obtained by using $S = 1 - \exp(-2r_a{}^2/\omega_a{}^2)$; where r_a indicates the aperture radius and ω_a indicates the beam radius at the aperture.

It is familiar that the embedded plasmonic nanoparticles in a glass matrix have strong NLO properties owing to the combination of electronic and thermal contributions, which are influenced by the pulse width and repetition rate of the femtosecond laser. The laser repetition rate of 80 MHz used in this, is the origin of thermal accumulation, hence both electronic and thermal contributions are sources of NLO properties. It is significant from the previous literature that the dipole oscillations in plasmonic nanoparticles produce a large local evanescent field in the vicinity of the NP surface even at non-resonant excitation (at 800 nm), thus the local field may add contribution to the NLO enhancement.

4. Conclusion

Glass doped with Cu NCs was successfully synthesized by an ion exchange method combined with an atmospheric post heat-treatment to produce spherical Cu NCs with sizes of 7–10 nm. XPS, Raman and XRD confirmed the formation of pure Cu and Cu_2O in the glass matrix after annealing. The Cu^+ ions were reduced to Cu^0 atoms by controlling the atmospheric post-heat treatment process. A blue shift of the SPR absorption peak was found to be ~5 nm after the post heat-treatment process. RBS measurements confirmed the Cu atoms near the glass surface after the ion exchange process and the diffusion of the Cu atoms into the glass matrix. The optical absorption spectroscopy and TEM measurements also confirmed the formation of spherical Cu NCs uniformly distributed near the glass surface. An increase in the size of the Cu NCs with an increase in annealing temperature was observed. Optical nonlinear absorption of the pristine and post heated Cu samples were analyzed by using a femtosecond laser Z-scan technique followed the excitation closer to the plasmon resonance of the Cu NCs. The annealed samples demonstrated large third order nonlinearities even at low excitation intensities. The large nonlinearities could be due to the influence of thermal nonlinearity along with electronic nonlinearity since a larger number of pulses (80 MHz) per second were interacting with the sample at the same place which possibly resulted in heating of the sample. The results show that the γ, β and $\chi^{(3)}$ of the glass doped with Cu NCs are -1.72×10^{-17} m^2/W, 9.96×10^{-11} m/W, 0.56×10^{-11} esu, which shows a good NLO behavior with possible applications in the field of nonlinear optics. Therefore, the glasses doped with noble metal NCs may have potential applications in optical limiting, object's contrast enhancement and the field of nonlinear optics with further improvement.

Acknowledgements

This work is based on the research supported by the South African Research Chairs Initiative of the Department of Science and Technology (84415) and the National Research Foundation (Prof. R.E. Kroon, Grant Number 93214) for photoluminescence measurements.

Appendix A. Supplementary data

Supplementary data associated with this article can be found, in the online version, at doi:10.1016/j.apmt.2019.02.016.

References

[1] P.N. Prasad, D.J. Williams, Introduction to Nonlinear Optical Effects in Molecules and Polymers, Wiley, New York, 1990.
[2] W. Koechner, Solid-State, Laser Engineering, vol. 1, 3rd ed., Springer Ser. Opt. Sci., Springer, Berlin, Heildelberg, 1992.
[3] G.I. [3] Stegeman, A. Miller, in: J. Michninter (Ed.), InPhotonic Switching, vol. 1, Academic, Orlando, 1992, pp. 81–146.
[4] H. Zhang, D.E. Zelmon, L. Deng, H.K. Liu, B.K. Teo, Optical limiting behavior of nanosized polyicosahedral gold-silver clusters based on third-order nonlinear optical effects, J. Am. Chem. Soc. 123 (2001) 11130–11300.
[5] R. Philip, P. Chantharasupawong, H. Qian, R. Jin, J. Thomas, Evolution of nonlinear optical properties: from gold atomic clusters to plasmonic nanocrystals, Nano Lett. 12 (2012) 4661–4667.
[6] R. Philip, G.R. Kumar, N. Sandhyarani, T. Pradeep, Picosecond optical nonlinearity in monolayer-protected gold, silver, and gold-silver alloy nanoclusters, Phys. Rev. B 62 (2000) 13160–13166.
[7] C. Zheng, Y. Du, M. Feng, H. Zhan, Shape dependence of nonlinear optical behaviors of nanostructured silver and their silica gel glass composites, Appl. Phys. Lett. 93 (2008) 143108.
[8] K. Wang, H. Long, M. Fu, G. Yang, P. Lu, Size-related third-order optical nonlinearities of Au nanoparticle arrays, Opt. Express 18 (2010) 13874–13879.
[9] P. Prem Kiran, B.N.S. Bhaktha, D. Narayana Rao, Nonlinear optical properties and surface-plasmon enhanced optical limiting in Ag–Cu nanoclusters co-doped in SiO_2 Sol-Gel films, J. Appl. Phys. 96 (2004) 6717–6723.
[10] R. Sreeja, R. Reshmi, P.M. Aneesh, M.K. Jayaraj, Liquid phase pulsed laser ablation of metal nanoparticles for nonlinear optical applications, Sci. Adv. Mat. 4 (2012) 439–448.
[11] R.F. Haglund Jr., Li. Yang, Nonlinear optical properties of metal-quantum-dot composites synthesized by ion implantation, Nucl. Instrum. Methods Phys. Res. Sect. B: Beam Interact. Mater. Atoms 91 (1994) 493–504.
[12] T. Cesca, P. Calvelli, G. Battaglin, P. Mazzoldi, G. Mattei, Local-field enhancement effect on the nonlinear optical response of gold-silver nanoplanets, Opt. Express 20 (2012) 4537–4547.
[13] R.F. Haglund Jr., Ion implantation as a tool in the synthesis of practical third-order nonlinear optical materials, Mater. Sci. Eng. A 253 (1998) 275–283.
[14] L. Francois, M. Mostafavi, J. Belloni, Optical limitation induced by gold clusters. 1. Size effect, J. Phys. Chem. B 104 (2000) 6133–6137.
[15] K. Fukumi, A. Chayahara, K. Kadono, Au^+-ion-implanted silica glass with non-linear optical property, Japan. J. Appl. Phys. 30 (1991) L742–L744.
[16] H. Tsuji, S. Kido, Y. Gotoh, J. Ishikawa, Negative-ion implanter for powders and its application to nanometer-sized metal particle formation in the surface of glass beads, Rev. Sci. Instr. 71 (2000) 804–806.
[17] R. Magruder, Li. Yang, Haglund Jr., C. White, L. Yang, R. Dorsinville, R. Alfano, Optical properties of gold nanocluster composites formed by deep ion implantation in silica, Appl. Phys. Lett. 62 (1993) 1730–1733.
[18] P. Kumar, M.C. Mathpal, H.C. Swart, Multifunctional properties of plasmonic Cu nanoparticles embedded in a glass matrix and their thermodynamic behavior, J. Alloy Compd. 747 (2018) 530–542.
[19] O.C. Mukhoro, W.D. Roos, M. Jaffer, J.J. Bolton, M.J. Stillman, D.R. Beukes, E. Antunes, Very green photosynthesis of gold nanoparticles by a living aquatic plant: photoreduction of Au by the seaweed, Chem. – A Eur. J. 24 (7) (2018) 1657–1666.
[20] S. Hamad, P.G. Krishna, S.P. Tewari, S. Venugopal Rao, Influence of picosecond multiple/single line ablation on Copper nanoparticles and nanostructures fabricated for surface enhanced Raman spectroscopy and photonics applications, J. Phys. D: Appl. Phys. 46 (2013) 485501–485514.
[21] S. Venugopal Rao, Picosecond nonlinear optical studies of gold nanoparticles synthesized using coriander leaves, J. Modern Opt. 58 (2011) 1024–1029.
[22] S. Venugopal Rao, T. Shuvan Prashant, T. Sarma, P.K. Panda, D. Swain, S.P. Tewari, Two-photon and three-photon absorption in dinaphthaporphycenes, Chem. Phys. Lett. 514 (2011) 98–103.
[23] S. Hamad, S.P. Tewari, L. Giribabu, S. Venugopal Rao, Picosecond and Femtosecond optical nonlinearities of novel corroles, J. Porphy. Phth. 16 (2012) 140–148.
[24] M. Sheik-Bahae, A.A. Said, T.H. Wei, D.J. Hagan, E.W. Van Stryland, Sensitive measurement of optical nonlinearities using a single beam, IEEE J. Quant. Electron. 26 (1990) 760–764.
[25] V.S. Jadhav, A. Bankar, S. Zinjarde, V.N. Bhoraskar, S.D. Dhole, Size control of Cu nanoparticles in ion-exchanged soda-lime glass by 6 MeV electron irradiation and its application in biofilm inhibition, Int. J. Green Nanotechnol. 4 (2012) 455–463.
[26] D. Manikandan, S. Mohan, K.G.M. Nair, Optical absorption of copper nanocluster composite soda-lime glass synthesized by binary ion-exchange and ion irradiation, Mater. Lett. 58 (2004) 907–910.
[27] M.C. Mathpal, P. Kumar, R. Balasubramaniyan, J.S. Chung, A.K. Tripathi, M.K. Singh, M.M. Ahmad, S.N. Pandey, A. Agarwal, Ag/TiO_2/graphene stacking for plasmonic metamaterial-based transparent semiconducting thin films, Mater. Lett. 128 (2014) 306–309.
[28] D. Manikandan, S. Mohan, P. Magudapathy, K.G.M. Nair, Blue shift of plasmon resonance in Cu and Ag ion-exchanged and annealed soda-lime glass: an optical absorption study, Phys. B 325 (2003) 86–91.
[29] U. Kreibig, M. Vollmer, Optical Properties of Metal Clusters, Springer-Verlag, Germany, 1995.
[30] D. Gall, Electron mean free path in elemental metals, J. Appl. Phys. 119 (2016) 085101–085105.
[31] R. Debnath, S.K. Das, Site-dependent luminescence of Cu^+ ions in silica glass, Chem. Phys. Lett. 155 (1989) 52–58.
[32] Y. Xiu-Chun, Influences of ion exchange and thermal treatment on photoluminescence of noble metal doped silicate glasses, J. Inorg. Mater. 31 (2016) 1039–1045.
[33] D. Manikandan, S. Mohan, K.G.M. Nair, Photoluminescence of embedded copper nanoclusters in soda-lime glass, Mater. Lett. 57 (2003) 1391–1394.
[34] Y. Qiao, D. Chen, X. Liu, J. Ruan, J. Qiu, T. Aka, Blue green emission from a Cu-doped transparent material prepared by sintering porous glass, IEEE Photonic Technol. Lett. 20 (2008) 1390–1392.
[35] H.S. Carranco, G.J. Dıaz, A.E. Garcıa, M.B. Garcıa, M.G. Arellano, J.M. Juarez, G.R. Paredes, R.P. Sierra, Photoluminescence and X-ray diffraction studies on Cu_2O, J. Lumin. 129 (2009) 1483–1487.
[36] P. Colomban, H.D. Schreiber, Raman signature modification induced by copper nanoparticles in silicate glass, J. Raman Spectrosc. 36 (2005) 884–890.
[37] P. Manikandan, D. Manikandan, E. Manikandan, A. Christy Ferdinand, Structural, optical and micro-raman scattering studies of nanosized copper ion (Cu^+) exchanged soda lime glasses, Plasmonics 9 (2014) 637–643.
[38] P. Colomban, Polymerization degree and Raman identification of ancient glasses used for jewelry, ceramic enamels and mosaics, J. Non-Cryst. Sol. 323 (2003) 180–187.
[39] W. Xiang, H. Gao, Li Ma, Xin Ma, Y. Huang, L. Pei, X. Liang, Valence state control and third-order nonlinear optical properties of copper embedded in sodium borosilicate glass, ACS Appl. Mater. Interfaces 7 (2015) 10162–10168.
[40] R.W. Boyed, Nonlinear Optics, 3rd ed., Elsevier Inc., 2008.
[41] K. Wang, H. Long, M. Fu, G. Yang, P.X. Lu, Intensity-dependent reversal of nonlinearity sign in a gold nanoparticle array, Opt. Lett. 35 (2010) 1560–1562.
[42] Y. Gao, X. Zhang, Y. Li, H. Liu, Y. Wang, Q. Chang, W. Jiao, Y. Song, Saturable absorption and reverse saturable absorption in platinum nanoparticles, Opt. Commun. 251 (2005) 429–433.
[43] M. Samoc, A. Samoc, B.L. Davies, H. Reisch, U. Scherf, Saturable absorption in poly(indenofluorene):a picket-fence polymer, Opt. Lett. 23 (1998) 1295–1297.
[44] M. Rumi, J.W. Perry, Two-photon absorption: an overview of measurements and principles, Adv. Opt. Photon. 2 (2010) 451–518.
[45] N. Venkatram, D.N. Rao, M.A. Akundi, Nonlinear absorption, scattering and optical limiting studies of CdS nanoparticles, Opt. Express 13 (2005) 867–872.
[46] B. Gu, W. Ji, Two-step four-photon absorption, Opt. Express 16 (2008) 10208–10213.
[47] K.V. Saravanan, K.C. James Raju, M.G. Krishna, S.P. Tewari, S. Venugopal Rao, Large three-photon absorption in $Ba_{0.5}Sr_{0.5}TiO_3$ films studied using Z-scan technique, Appl. Phys. Lett. 96 (2010) 232905.
[48] D.S. Correa, L.D. Boni, L. Misoguti, I. Cohanoschi, F.E. Hernandez, C.R. Mendonca, Z-scan theoretical analysis for three, four- and five-photon absorption, Opt Commun. 277 (2007) 440–445.